Journal of Thermal Analysis and Calorimetry, Vol. 74 (2003) 41–56

DSC STUDY OF PRECIPITATION PROCESSES IN Cu–Co–Si ALLOYS

A. Varschavsky and E. Donoso[*]

Universidad de Chile, Facultad de Ciencias Físicas y Matemáticas, Instituto de Investigaciones y Ensayes de Materiales, IDIEM, Casilla 1420, Plaza Ercilla 883, Santiago, Chile

(Received June 12, 2002; in revised form March 3, 2003)

Abstract

Using differential scanning calorimetry (DSC) the precipitation processes of supersaturated solid solutions of three Cu–Co–Si alloys containing the same atomic cobalt content were investigated. Thermoanalytical and previous studies, reveal that the decomposition begins with cobalt clustering which initiates the precipitation of the Co_2Si stoichiometric particles, which in turn dissolves after further heating. Volume fractions are unequivocally determined by the amount of cobalt present in these alloys. It is infered that surplus silicon atoms retained in the solution increase the reaction rate and dispersity of precipitate structure. Kinetic parameters were obtained by a convolution method based in the Mehl–Johnson–Avrami (MJA) formalism. The lower activation energy associated with cobalt clustering is attributed to the contribution of quenched-in vacancies. Superimposed to the MJA formalism and adaptative spherical diffusion model was used for Co_2Si precipitation with particle size as a disposable parameter. This model further confirmed that as silicon content increases particle dispersity becomes more pronounced. Such results are also infered from a three dimensional diffusion dissolution model previously developed which adjusts quite well to such process in the present cases. Age hardening experiments are in line with all previous results obtained.

Keywords: cobalt, copper, diffusion, kinetics, precipitation, silicon

Introduction

For the past several years attempts have been made to produce ternary alloys with desirable combinations of mechanical properties and microstructural stability. For instance since the early work of Corson [1] the precipitation processes and the precipitation hardening in Cu–Co–Si alloys have been investigated by several authors [2–8]. It has been established that the orthorhombic Co_2Si phase is the equilibrium precipitate phase [1–3, 5, 6, 9]. Also, in presence of Co_2Si particles the solid solubilities of cobalt and silicon were also afterwards studied. In others investigations on Cu–Co–Si alloys the precipitation processes were investigated by electrical resistivity [8, 10, 11], thermoelectric power [8, 11] and differential scanning calorimetry (DSC) [11,

* Author for correspondence: E-mail: edonso@cec.uchile.cl

1388–6150/2003/ $ 20.00

Akadémiai Kiadó, Budapest
Kluwer Academic Publishers, Dordrecht

12]. These last studies justified the mechanical behavior of the alloys and have also given information about the nucleation and growth of the stable Co_2Si precipitates. Previous authors works [13, 14] were concerned with the fatigue behavior of some Cu–Co–Si alloys of quasi-binary compositions Cu–$x$$Co_2Si$.

Chiefly, the present work was performed in order: a) to evaluate the precipitation processes of Co_2Si particles starting from a supersaturated solid solution of Cu–Co–Si alloys containing approximately the same amount of cobalt but different amounts of surplus silicon with respect to the stoichiometric Co_2Si composition, using differential scanning calorimetry; b) to assess the kinetics of precipitation by determining the kinetic parameters via a convolution method to give account of overlapping effects; c) to superimpose to the kinetic curves a diffusion kinetic mechanism which gives account of the diffusion of silicon in cobalt in order to explain Co_2Si formation stage displayed by the DSC curves; d) to evaluate precipitate dissolution via a three-dimensional diffusion model and e) to search for the aging behavior of the alloys.

Experimental method

The composition of the alloys investigated is listed in Table 1. It is worth noticing that the alloy A corresponds to the quasi-binary Cu–1 at% Co_2Si alloy. The alloys were prepared in vacuum in a Baltzers VSG-10 induction furnace, from electrolytic copper (99.95% purity), and master alloys of Cu–10 mass% Co and Cu–15 mass% Si.

Table 1 Alloys composition

Alloy designation	Co/at%	Si/at%
A	0.65	0.33
B	0.65	0.86
C	0.66	1.1

The ingots were forged at 1273 K to a thickness of 20 mm, afterwards they were annealed at 1273 K during 72 h to achieve complete homogenization and furnace-cooled to room temperature. Subsequently the materials were cold-rolled to a thickness of 2 mm with intermediate annealings of 1 h at 1073 K.

After the last anneal the alloys were water quenched. Calorimetric measurements were carried out in a DuPont 2000 thermal analyser at heating rates ϕ, of 0.033, 0.083, 0.167, 0.333 and 0.833 K s^{-1}. To increase the sensitivity of the measurements, a high purity, well annealed copper disc, was used as a reference. In order to minimize oxidation argon ($0.8 \cdot 10^{-4}$ m^3 min^{-1}) was passed through the calorimeter.

Runs were recorded between 300 and 950 K. After the first run specimens of alloys A, B and C were maintained at 850, 780 and 750 K respectively for 5 min and allowed to cool freely in the calorimeter for 3 h yielding cooling curves that were very similar and nearly exponential. It was observed for all specimens that the cooling rate lied between 0.48 and 0.417 K s^{-1} in this temperature range and 0.117 K s^{-1} below

560 K. When room temperature was reached, a second run at the same heating rate was made by heating specimens of alloys A, B and C up to 850, 780 and 750 K respectively in order to avoid displayement of the Co_2Si dissolution reaction. The DSC traces presented in this work were obtained by subtracting the baseline from the first run. This baseline represents the temperature-dependent heat capacity of the alloys in the existing thermal conditions, and its value was in agreement with the Kopp-Neumann rule. Afterwards, the resulting traces were converted into a differential heat capacity *vs*. temperature curve. The remaining heat-capacity, namely the differential heat capacity ΔC_p represents the heat associated with solid state reactions during the DSC run. Thus, reaction peaks in the ΔC_p *vs. T* curve can be characterized by the reaction enthalpy of a particular event. The DSC curves presented in this work are all such rerun-corrected curves.

Results and discussion

The DSC curves

In Fig. 1 DSC curves obtained at the indicated heating rates on quenched samples of alloys A, B and C are shown. The DSC curves reveal two distinct exothermal peaks, stage 1 and 2, which overlap more as the silicon content increase. It has been shown [11, 15] that stage 1 and 2 can be associated to Co and Co_2Si precipitates formation respectively. An endothermic peak designated as stage 3 is associated with the dissolution of the Co_2Si particles, as its heat content value is approximately equal to that of stage 2 for each alloy at the same heating rate ϕ. In Table 2 are listed the heat involved in the three stages.

It can also be observed a small decrease of the heats associated to all stages measured by the area under the peaks as ϕ increases. This effect is not considerable, but in all cases it can be attributed to the fact that heating takes place in a higher temperature range as related to the Co and Co_2Si solvus with increasing ϕ values. The same effect in stage 3 is a consequence of the lower of heat content of stage 2 for larger values of ϕ.

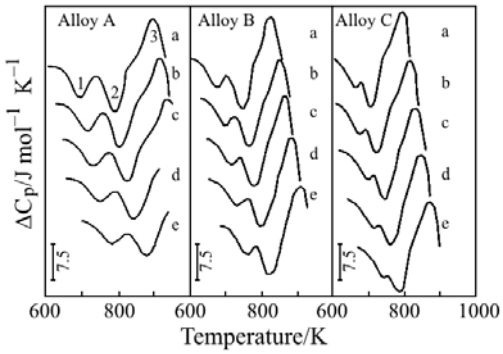

Fig. 1 DSC traces for quenched alloys under study where the three main heat effects are shown. Heating rates are: a – 0.033 K s^{-1}; b – 0.083 K s^{-1}; c – 0.167 K s^{-1}; d – 0.333 K s^{-1}; e – 0.833 K s^{-1}

Table 2 Reaction heats involved in the different stages associated with the linear heating experiments (J mol^{-1})

ϕ/K s^{-1}	Alloy A			Alloy B			Alloy C		
	Stage 1	Stage 2	Stage 3	Stage 1	Stage 2	Stage 3	Stage 1	Stage 2	Stage 3
0.033	339	585	580	342	583	577	335	585	579
0.083	333	577	570	335	575	568	328	581	575
0.167	325	563	558	330	567	563	318	568	561
0.333	320	554	547	323	556	555	315	558	553
0.833	315	545	538	318	548	544	308	546	544

An important effect is the shift to lower temperatures which exhibit all stages when the silicon concentration increases as shown in Fig. 2 for the employed values of ϕ. Precipitation of cobalt at decreasing temperatures shown by the shift of peak temperatures for higher silicon contents in Fig. 2a, might be due to the shift of the solvus to the left, thus increasing the supersaturation of the solid solution, leading therefore to a decrease in the critical nuclei and to an increase in the reaction rate and dispersity of the precipitates. In fact as volume fraction of precipitates is controlled by cobalt concentration, which is the same for the three alloys, an increase of dispersity means a smaller particle radii in conjuction with a higher particle density. The larger thermal event shift to lower temperatures is evidenced for stage 2 in Fig. 2b by the decrease of peak temperatures as silicon content increases; this implies a larger reaction rate. In fact if such rate is controlled mainly by the diffusion silicon in copper, the value of the diffusion coefficient is enhanced as silicon concentration is increased. This feature will be treated later on. Figure 2c shows also a decrease in peak temperatures for stage 3 as the alloy is reacher in silicon. This fact also implies that the onset of peak dissolution temperatures T_{03}, decrease, which in turn means that finer precipitates are dissolving, The observed decrease in precipitate stability is a consequence of their larger surface to volume ratio as particles became smaller.

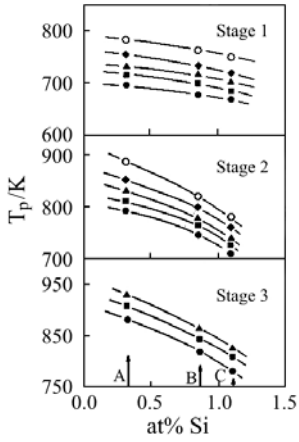

Fig. 2 Peak temperatures of the main heat effects for alloys A, B and C *vs.* silicon content. Heating rates are: ● – 0.033 K s^{-1}; ■ – 0.083 K s^{-1}; ▲ – 0.167 K s^{-1}; ◆ – 0.333 K s^{-1}; ○ – 0.833 K s^{-1}

If the molar dissolution entropy is evaluated as:

$$\Delta S_p = \frac{\Delta H_p}{T_{03}} \tag{1}$$

being ΔH_p=221.6 kJ mol^{-1} the molar dissolution enthalphy of the precipitates [15], values of ΔS_p=0.27/0.28/0.32 J mol^{-1} K^{-1} are obtained for alloy A, B and C taking T_{03}=826/765/716 K. It should be noticed that T_{03} values were computed as $\phi \rightarrow 0$,

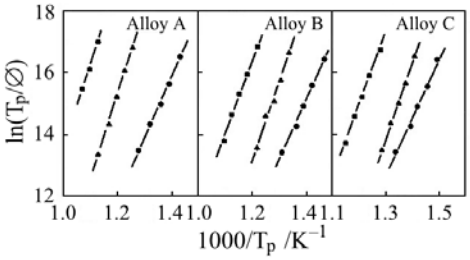

Fig. 3 Modified Kissinger plots for the different DSC stages in quenched alloys A, B and C. ● – stage 1; ▲ – stage 2; ■ – stage 3

which in turn were obtained from extrapolation of onset temperatures for decreasing ϕ values. These sort of computations were made in order to avoid heating rate effects.

The small increase in molar dissolution entropy is the reflection of the larger amount of internal order exhibiting those precipitates corresponding to increasingly silicon concentration in line with their infered smaller size. This feature is in agreement with a less fault probability exhibited by smaller sized particles.

The fact that the heat contents of stages 1, 2 and 3 are the same for alloys A, B and C for a certain ϕ value implies, as said before, that the cobalt content controls the amount of Co_2Si and that this amount is equal for the three alloys in this case. Since alloy A is the quasi-binary Cu–1 at% Co_2Si, the surplus silicon concentration over this composition remains in solution. It should obviously be pointed out that this effect holds providing there is enough silicon to form Co_2Si compound.

An other general result obtained from the DSC traces is the evaluation of precipitate volume fractions V_f given by the expression:

$$V_f = \frac{\Delta H_3}{\Delta H_p} \frac{\rho_s}{\rho_p} \tag{2}$$

in which ΔH_3 is the dissolution heat when $\phi \rightarrow 0$ extrapolated from the curves ΔH_3 *vs.* ϕ in order to avoid again heating rate effects, ρ_s and ρ_p are the alloy and precipitate densities respectively.

On calculating ΔH_3=584/579/582 J mol^{-1}, ρ_s=8.94/8.92/8.89 kg m$^{-3}\cdot 10^3$ for alloys A, B and C, being ρ_p=6.71·10^3 kg m$^{-3}\cdot 10^3$ one computes approximately V_f=3.5·10^{-3} for the three alloys approximately, a value which is in line with the previous results given in connection with the cobalt concentration control on the precipitation processes.

In closing this section it is worth noticing the rather skewed shape of the dissolution peaks during the DSC runs in Fig. 1. The slow reaction rate at the early stages is due to the combined effects of a slow diffusion rate because of the low temperatures, the small concentration gradient near the particle-matrix interface and the relatively small interfacial area to particle volume ratio. The dissolution rate is increasing as temperature is rising and towards the end of the dissolution process the rate is very high. This is because the combined effect of a high diffusion rate, the large concentration gradient near the in-

terface and the high ratio of interface area to particle volume. It is also expected that the particle size affects the kinetics of dissolution. Small particles should trend to shift the peak to smaller temperatures and are fully dissolved in a shorter time, while increasing particle radius shift the peak to higher temperatures. A smaller particle size corresponds to a higher particle density for a fixed volume fraction of particles. In this way, the diffusion distances are smaller and the reaction reaches completion faster.

Precipitation kinetics

To study the precipitation kinetics of the present reactions, activation energies E were calculated by a modified Kissinger method [16]:

$$\ln\left(\frac{T_p^2}{\phi}\right)=\frac{E}{RT_p}+\ln\left(\frac{E}{Rk_0}\right) \tag{3}$$

where T_p is the peak temperature, k_0 a pre-exponential factor and R the gas constant. Therefore E and also k_0 can be obtained from a plot $\ln(T_p^2/\phi)$ *vs.* $1/T_p$ as shown in Fig. 3. Values of E and k_0 are independent of the kinetic model chosen provided T_p is the peak temperature [16]. In Table 3 one can read the respective values of the activation energies and pre-exponential factors. It can be infered that the values of activation energies resulted somewhat larger than those reported by Lendvai *et al*. [11].

Utilizing Brown and Ashby [17] and also Shi *et al*. [18] correlations, an activation energy for diffusion of cobalt in copper E_{Cu}^{Co}=203.5 kJ mol^{-1} was estimated resulting much higher than the calculated values for stage 1. This fact can be attributed to the strong contribution of quenched in vacancies, with an activation energy for migration of about one half of the above value. The measured activation energies for stage 1 also do not vary for the three alloys as can be expected since cobalt composition is the same and also because silicon diffusion is mainly not involved in this stage. It can be demonstrated that although quenched-in vacancies play an important role in cobalt precipitation, their annihilation effect makes a negligible contribution to evolved heat ΔH_1. The fraction of ΔH_1 associated with vacancy annihilation f_v, can be readily obtained as:

$$f_v=\exp\left(\frac{\Delta S_k}{R}\right)\exp\left(-\frac{\Delta H_f}{RT_q}\right)\frac{\Delta H_f}{\Delta H_1}$$

where ΔH_f=106.4 kJ mol^{-1} [19] is the vacancy formation energy, ΔS_k=5.76 J mol^{-1} K [20], ΔH_1=340 J mol^{-1} and T_q=1073 K the quenching temperature.

Values of f_v=4.1·10^{-3} are obtained as an average for alloys A, B and C which as said before is negligible. For stage 2, since the apparent activation energy is a weighted value between that of silicon in cobalt and silicon in copper, and as the volume of Co_2Si particles is small when compared to that of the bulk material, the measured activation energies should be essentially similar to that of silicon in copper. In the range of silicon concentrations here considered from [17, 18] only an estimated value E_{Cu}^{Si}=202 kJ mol^{-1} can be given. In fact for this small range of concentrations, individual values for the activation

Table 3 Activation energies and pre-exponential factors for the three alloys under study

	Alloy A			Alloy B			Alloy C		
	Stage 1	Stage 2	Stage 3	Stage 1	Stage 2	Stage 3	Stage 1	Stage 2	Stage 3
E/kJ mol^{-1}	155.6	208.2	198.2	153.8	203.7	194.4	152.1	197.2	189.8
k_0/s^{-1}	$6.6\cdot 10^{8}$	$4.3\cdot 10^{11}$	$6.5\cdot 10^{9}$	$3.1\cdot 10^{8}$	$5.0\cdot 10^{10}$	$3.1\cdot 10^{9}$	$1.2\cdot 10^{8}$	$1.5\cdot 10^{10}$	$6.0\cdot 10^{9}$

energies for diffusion can not be distinguished each other for the three alloys. In the present case it is however expected a decrease in activation energy as the silicon content increases [17, 18]. This feature can be attributed to the fact that the average temperature values between the liquidus and the solidus for a given concentration strongly decrease when silicon concentration increases in larger extents. This tendency is also observed in our results in spite that the range of silicon variation is small in the alloys under study. A value E_3=199 kJ mol^{-1} can be calculated which is close to the similar values for E_{Cu}^{Co} and E_{Cu}^{Si} computed from [17, 18], although a trend to become lower with silicon content increase is observed. Such tendency is expected in connection with the same arguments given for the activation energy decrease in stage 2. The larger the pre-exponential factor for stage 1 for lower silicon contents implies that the jump rate of atoms across the particle-bulk interface increase, thus decreasing the dispersity of precipitation [21].

The kinetic analysis for stages 1 and 2 for the three alloys under study was performed according to Mehl–Johnson–Avrami equation ussually used for heterogeneous reactions (as they are in the present case) under non isothermal conditions

$$y=1-\exp[-(k_0\theta)^n] \tag{4}$$

where 'y' is the reacted fraction, k_0 a pre-exponential factor,

$$\theta=\frac{T^2R}{\phi E}\exp\left(-\frac{E}{RT}\right) \tag{5}$$

is the reduced time [22, 23], and n a constant.

If two DSC peak overlap each other, such is the situation for Co and Co_2Si formation, the total heat flow $\Delta\dot{H}_T$ per unit mass at any time/temperature can be expressed as the sum of the heat flow of the individual transformation $\Delta\dot{H}_1$ and $\Delta\dot{H}_2$ as [21]

$$\Delta\dot{H}_T=\Delta\dot{H}_1+\Delta\dot{H}_2=A_1\dot{y}_1+A_2\dot{y}_2 \tag{6}$$

In this equation A_1 and A_2 are the areas of the individual peaks, while $\dot{y}_1$ and $\dot{y}_2$ are the transformation rates, being easily derived for each reaction form Eq. (4) as:

$$\left(\frac{dy}{dt}\right)=nk_0^n\theta^{n-1}\frac{d\theta}{dt}\exp[-(k_0\theta)^n]$$

which, with the aid of Eq. (5), becomes:

$$\dot{y}=nk_0^n\left(\frac{T^2R}{\phi E}\right)^{n-1}\exp\left(-\frac{nE}{RT}\right)\exp\left[-k_0^n\left(\frac{T^2R}{\phi E}\right)^n\exp\left(-\frac{nE}{RT}\right)\right] \tag{7}$$

From Eq. (6), after assigning to reactions 1 and 2 the respective subscripts, one finally obtain

$$\dot{H}_T=\sum_{i-1}^{2}A_i n_i k_0^n\left(\frac{T^2R}{\phi E_1}\right)^{n_1-1}\exp\left(-\frac{nE}{RT}\right)\exp\left\{-\left[\left(\frac{T^2R}{\phi E}\right)^n\exp\left(-\frac{n_1E_1}{RT}\right)\right]\right\} \tag{8}$$

The area of the individual peaks must add up the total area $A=A_1+A_2$. This equation is identical to that obtained previously by Borrego *et al*. [24, 25] working with $k_0\theta$ as a state variable and later on by the authors working with the reduced time [15].

By fitting this equation to the experimental heat flow data $\Delta\dot{H}_T$ employing computerized methods of minimization of least squares error, the parameters n_1 and n_2 can be obtained, which in conjunction with the apparent activation energies for stages 1 and 2 and the respective pre-exponential factors calculated from the modified Kissinger method shown in Table 2, constitute the kinetic parameters for each individual reaction. Exponents n_1 and n_2 are listed in Table 4.

Table 4 Values of the Mehl–Johnson–Avrami exponents

	Alloy A		Alloy B		Alloy C	
	Stage 1	Stage 2	Stage 1	Stage 2	Stage 1	Stage 2
n_1	1.13		1.16		1.14	
n_2		1.48		1.58		1.51

Also parameters A_1 and A_2 can be calculated in each case and hence, since heat flow per unit mass of the sample $\Delta\dot{H}=\Delta C_p\phi/MW_s$ where MW_s is the molecular mass of the precipitate ($=58.93\cdot10^{-3}/48.65\cdot10^{-3}$ kg mol^{-1}, for Co and Co_2Si respectively) the associated reaction heats associated to stages 1 and 2 can be readily obtained. For instance, respective values for alloy A are 320 and 569 J mol^{-1}. The fit of the calculated to the experimental curve for this alloy is shown in Fig. 4 for ϕ=0.17 K s^{-1}. In this figure the experimental curve, the adjusted curve and the individual curves corresponding to each stage are plotted. These values are in fairly good concordance with those obtained from the energetics of both processes. Similar curves were obtained for the other two alloys, not shown here for brevity sake.

The values of n_1 are closely indicative of a process of nucleation and growth (n=1), although some precipitation could be taken place during quenching, while those for n_2 are nearly indicative of a process of growth from pre-existing nucleus of non-negligible size (n=1.5) [26].

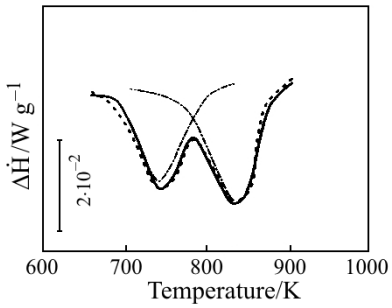

Fig. 4 Heat flow *vs.* temperature from DSC experiments at ϕ=0.167 K s^{-1} for alloy A. - – experimental composite curve; --- – calculated composite curve: · – · – – approximation to individual stages 1 and 2

Adaptative spherical diffusional model for stage 2

Along this research work and in agreement with literature [8, 15], stage 2 has been attributed to the formation of Co_2Si particles via diffusion of silicon into the precursory cobalt precipitates formed during stage 1. In the following we will adjust an adaptative model of diffusion of a component through a sphere maintaining the surface concentration constant, evaluating the concentration in its centre, which at the beginning of the reaction is assumed to be zero and equal to that of the surface when the reaction goes to completion. In this way the reacted fraction at the sphere centre is $y(0)=c_c/c_s$ where c_c is the instantaneous silicon concentration at the centre and c_s (=0.333) the constant concentration at the sphere surface. Such consideration neglects the sligth unavoidable overlapping of cobalt precipitation reaction with that for Co_2Si formation. If it is assumed that stage 2 follows this behaviour, the calculated values of $y(0)$ from this adaptative model can be superimposed, using the best fits to the Johnson–Mehl–Avrami kinetic paths at constant different temperatures, employing Co_2Si average particle radii 'a' as a disposable parameter. This treatment implies that the transferability principle is valid, that is, the kinetic parameters already calculated for non-isothermal conditions are the same as those for isothermal ones.

In fact, the diffusion equation in spherical coordinates is given by [27]:

$$\frac{\partial c}{\partial t}=D\left(\frac{\partial^2 c}{\partial r^2}+\frac{2}{r}\frac{\partial c}{\partial r}\right) \tag{9}$$

where D is the diffusion coefficient assumed to be constant, c the concentration and r the distance from the sphere center. The solution of this radial diffusion equation for the above boundary conditions gives for $y(r)=c/c_s$ [27]:

$$y(r)=1+\frac{2a}{\pi r}\sum_{n=1}^{\infty}\frac{(-1)^n}{n}\sin\frac{n\pi r}{a}\exp\left(-\frac{Dn^2\pi^2 t}{a^2}\right) \tag{10}$$

where 'a' is the sphere radius. The solution when $r\rightarrow 0$, yields for $y(0)=c_c/c_s$:

$$y(0)=1+2\sum_{n=1}^{\infty}(-1)^n\exp\left(-\frac{Dn^2\pi^2 t}{a^2}\right) \tag{11}$$

It is worth recalling that three parameters define the reacted fraction $y(0)$: E_{Co}^{Si}, D_0 and the disposable parameter 'a' in the present case. Values of $D=D_0\exp(-E_{Co}^{Si}/RT)$ should be computed. The isothermal temperatures were chosen in a range where no overlapping was observed in the non-isothermal runs when $\phi\rightarrow 0$. From Brown and Ashby correlations [17], a typical value of $D_0=0.1\cdot 10^{-4}$ m^2 s^{-1}; the activation energy for diffusion was estimated as $E_{Co}^{Si}=227.1$ kJ mol^{-1}, which is that of silicon in cobalt [17]. It was calculated that the increase of size which undergo the initial cobalt particle when the concentration of silicon reached at the centre correspond to that of the precipitate Co_2Si is about 14%, since the atomic size of silicon is similar to that of cobalt. Therefore the values of 'a' which satisfy the best fit of this model to the Mehl–Johnson–Avrami path are affected at the most by an error of about 7%. This treatment, although not so precise, avoid com-

plexities arising when moving boundary effects are considered. The results of the adjustment utilizing ten terms of the series contained in Eq. (11) are given at 780 K in Fig. 5 and at 820 K in Fig. 6, where particle radii obtained for the respective best fits are indicated for the three alloys. These values are in agreement with those observed by transmission electron microscopy for similar alloys compositions [11]. It should be also noticed that particle size decreases with the increase in silicon content, and that remains almost invariant when varying temperature. It is worth recalling that when calculating '*a*' values, the above treatment does not take into account the early simultaneous coarsening which can occur during the course of reaction. All these findings besides indicate that the diffusion parameters roughly resulted in a good selection.

The above results are also in line with those infered from the DSC curves regarding the increase in dispersity as the silicon content becomes larger, and that Co_2Si precipitates effectively form by the diffusion of silicon into the pre-existing cobalt precipitates grown during stage 1 of non-isothermal experiments. Such findings confirm at the same time that the values of the disposable parameter '*a*' allow to make both kinetic paths compatible as they fit quite well each other.

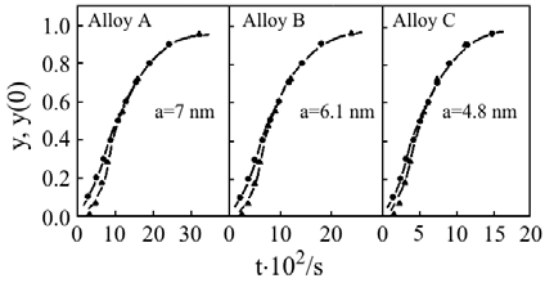

Fig. 5 Adjusted to reacted fraction *vs.* time of Mehl–Johnson–Avrami plots to the adaptative diffusion spherical model for the three alloys under study. Particle radii resulting for the best fits are indicated. *T*=780 K

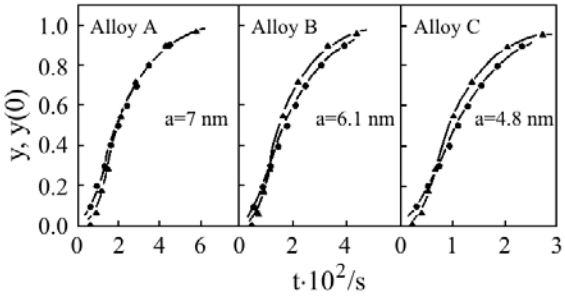

Fig. 6 The same as Fig. 5 for *T*=820 K

Precipitate dissolution kinetics

It was demonstrated in a previous work that in the quasi-binary Cu–1 at% Co_2Si (alloy A) the dissolution kinetics can be well adapted to the approach discussed in early

papers [28, 29]. In such approach three-dimensional controlled diffusion situations for spherical precipitates are described by means of the expression:

$$1-(1-y)^{2/3}=k_0\theta \tag{12}$$

where k_0 is a constant and θ is already defined.

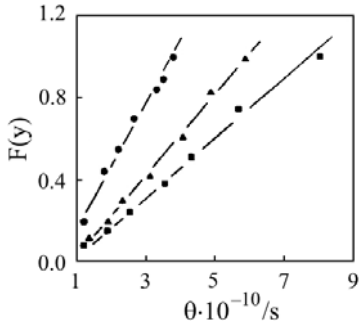

Fig. 7 Plots of the integrated kinetic function $F(y)=1-(1-y)^{2/3}$ *vs*. θ for the three alloys under study. ■ – alloy A; ▲ – alloy B; ● – alloy C

The results of plotting for stage 3 the left hand side term of Eq. (12), called integrated kinetic function, against θ for alloys A, B and C are shown in Fig. 7 for θ=0.033 K s^{-1}. It is clearly seen that the dissolution behaviour of Co_2Si precipitates is adjustable to this kinetic model for the three alloys under study, since straight lines of different slopes k_0 resulted in all cases. It was also demonstrated that in the present model that [28]:

$$k_0=\frac{k_0^*}{a^2} \tag{13}$$

where k_0^* is another constant. The results are summarized in Table 5, where particle radii 'a' were taken the same as those infered in the previous section.

Table 5 Values of constants k_0 obtained from plots in Fig. 7, particle radii and calculated values for k_0^* from Eq. (13)

	Alloy A	Alloy B	Alloy C
k_0/s^{-1}	$1.4\cdot 10^9$	$2\cdot 10^9$	$3\cdot 10^9$
a/m	$7\cdot 10^{-9}$	$6.1\cdot 10^{-9}$	$4.8\cdot 10^{-9}$
$k_0^*/m^2\ s^{-1}$	$6.9\cdot 10^{-8}$	$7.4\cdot 10^{-8}$	$6.9\cdot 10^{-8}$

It can be noticed the values of k_0 computed are of the same order of magnitude than those obtained from the modified Kissinger law of Eq. (3). Such findings also strongly suggest that k_0 values obtained from Eq. (3) are independent of the choice of the kinetic model as can be expected when temperature used in this equation is the peak temperature T_p [16].

When the values of '*a*' obtained in previous section are introduced in Eq. (13) it is noticed that k_0^* resulted nearly constant. In summarizing this section one can be assured from all these findings that the chosen model for the dissolution kinetics of Co_2Si particles is quite well satisfied. It also corroborates that particle size decrease as silicon content becomes larger. Besides, since volume fractions are the same for the three alloys, particle dispersity is increased as found before.

Ageing behavior

Figure 8 shows the hardness *vs*. time curves for the quenched alloys when ageing at 773 K. Curves for all alloys shift to higher hardness values with time and afterwards decrease because of the well known effect of overaging due to particle coarsening. Peak hardening is larger when silicon content increase as a consequence of dispersity of precipitates at constant volume fraction and to the larger surplus silicon contribution in solid solution. Peak hardening takes place earlier in alloy C followed by alloys B and A. This behavior is attributed to the increased precipitation kinetics of Co_2Si as alloys have larger silicon contents in line with the results obtained along this research work.

Conclusions

The precipitation and dissolution processes of Co_2Si particles were studied by differential scanning calorimetry (DSC) in three Co–Co–Si with a constant cobalt compo-

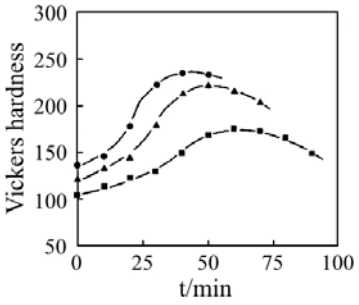

Fig. 8 Vickers microhardness *vs.* time after annealing 773 K for the three alloys. ■ – alloy A; ▲ – alloy B; ● – alloy C

sition. On the basis of the DSC curves it is infered (stage 2) that Co_2Si stoichiometric precipitates are formed by diffusion of silicon into the precursor clustering of cobalt atoms (stage 1) which nucleate and growth after quenching and heating linearly the supersaturated solid solutions. The silicon that is in excess to the composition of the stoichiometry Co_2Si remains in solution but a larger content in the initial supersaturated solid solution strongly enhances the nucleation of the particles, thus making finer the final structure. It is shown that the endothermic reaction displayed by the DSC curves (stage 3) correspond unequivocally to the dissolution of the Co_2Si precipitates and that precipitate volume fraction is determined by the amount of cobalt

present which was constant for the three alloys under study. It was also shown from molar dissolution entropy measurements that internal order becomes larger as particles are smaller. The kinetic parameters were determined using the Mehl–Johnson–Avrami formalism under non-isothermal conditions together with a convolution method based in the same formalism. The lower activation energy found for cobalt clustering is attributed to non-equilibrium vacancies contribution retained after the quench. Superimposed to the above kinetic path an alternative model was used in order to verify that Co_2Si particles can be formed as a consequence of diffusion of silicon in cobalt precursor spheres, employing particle size a disposable parameter. Such superimposed model also determines that a finer structure is also obtained as silicon content increases.

Precipitate dissolution kinetics adjusts perfectly to a three-dimensional diffusion kinetic law previously developed by the authors, confirming also the increasing dispersity of the structure with larger amounts of silicon. The same conclusion about particle dispersity is in line with results obtained from age hardening measurements. Peak hardening is higher and takes place faster for larger silicon contents under the same calculated precipitate volume fractions.

* * *

The authors wish to acknowledge the Fondo de Desarrollo Científico Technológico (FONDECYT), Proyect N° 1020127, for financial support, and the Facultad de Ciencias Físicas y Matemáticas, Universidad de Chile for the facilities provided for this research.

References

1 M. G. Corson, Rev. Metallurgia, 27 (1930) 265.
2 S. Gallo, Met. Italiana, (1958) 15.
3 N. I. Revina, A. K. Nikolahev and V. M. Rosenberg, Metalli, 17 (1975) 215.
4 V. F. Grabin and U. B. Malevsky, Metalloved. i Term. Obrakotka Metallov, 3 (1965) 28.
5 T. Toda, Trans. Jpn. Inst. Metals, 11 (1970) 24.
6 M. D. Teplitsky, A. K. Nikolahev, N. I. Revina and V. M. Rosenberg, Fizika Met. Metalloved, 40 (1975) 1240.
7 A. Korbel, W. Bochniak, A. Pawelek, F. Dobrzanski and H. Dybieh, Rudy i Metale Niezelarne, 25 (1980) 431.
8 B. Albert, Z. Metallk., 76 (1985) 528.
9 T. Toda and H. Takeuchi, J. Jpn. Inst. Metals, 11 (1970) 24.
10 B. Albert, Z. Metallk., 75 (1985) 475.
11 J. Lendvai, T. Ungar, I. Kovács and B. Albert, J. Mater. Sci., 23 (1988) 4059.
12 E. Donoso and A. Varschavsky, Anales del IX Congreso Internacional de Tecnología de Materiales y III Congreso Iberoamericano de Ingeniería Metalúrgica y de Materiales, Octubre 1994, Sao Paulo, Brasil, Vol. 2, p. 493.
13 A. Varschavsky and E. Donoso, Mater. Lett., 15 (1992) 207.
14 A. Varschavsky and E. Donoso, Anales del III Congreso Iberoamericano de Ingeniería Mecánica, Septiembre 1997, La Habana, Cuba, Vol. 1, p. 119.
15 A. Varschavsky and E. Donoso, J. Therm. Anal. Cal., 68 (2002) 231.

16 E. J. Mittemeijer, Lui Cheng, P. J. Van der Shaaf, C. M. Brakman and B. M. Korevaar, Metall. Trans., 19 A (1988) 925.
17 A. M. Brown and M. F. Ashby, Acta Metall., 28 (1980) 1085.
18 F. J. Shi, T. G. Nieh and Y. T. Chou, Scripta Mater., 43 (2000) 265.
19 E. Donoso and A. Varschavsky, J. Thermal Anal., 45 (1995) 1419.
20 A. Varschavsky and M. Pilleux, Mater. Letts., 17 (1993) 364.
21 R. F. Speyer, B. C. Richardson and S. H. Risbud, Metall. Trans., 17 A (1986) 1479.
22 A. Varschavsky, Thermochim. Acta, 203 (1992) 391.
23 A. Varschavsky and J. Sesták, in Characterization Techniques of Glasses and Ceramics, J. M. Rincón and M. Romero, Eds Springer, N. Y. 1999, p. 85.
24 A. Borrego and G. González-Docel, Mater. Sci. Eng., A245 (1998) 10.
25 A. Borrego and G. González-Docel, Mater. Sci. Eng., A276 (2000) 292.
26 J. W. Christian, The Theory of Transformation of Metals and Alloys, 2nd Ed., Pergamon Press, England 1971, p. 534.
27 J. Crank, The Mathematics of Diffusion, Oxford University Press, London (England) 1976, pp. 84, 86.
28 A. Varschavsky and E. Donoso, Thermochim. Acta, 69 (1983) 341.
29 A. Varschavsky and E. Donoso, J. Mater. Sci., 21 (1986) 3873.